



## Preparation and Application of $\text{ZnFe}_2\text{O}_4/\alpha\text{-Al}_2\text{O}_3$ for Photocatalytic Degradation of Methylene Blue Dye and Real Textile Effluent

Alhaji Saleh Zanna Umara<sup>1</sup>, Abdulhamid Hamza<sup>2\*</sup>, Diya'uddeen Basheer Hasan<sup>3</sup>

<sup>1</sup> Department of Industrial and Environmental Technology, National Research Institute for Chemical Technology Zaria, Nigeria

<sup>2</sup>Department of Chemical Engineering, Ahmadu Bello University Zaria, Nigeria

<sup>3</sup>Center for Energy Research and Training, Ahmadu Bello University Zaria, Nigeria

\*Corresponding author : ahamza@abu.edu.ng

Received : 02 October 2018

Accepted : 07 August 2019

Online : 31 August 2019

**Abstract** – Present work was aimed at the development of  $\alpha\text{-Al}_2\text{O}_3$  supported  $\text{ZnFe}_2\text{O}_4$  visible-light responsive photocatalysts.  $\text{ZnFe}_2\text{O}_4$  and  $\alpha\text{-Al}_2\text{O}_3$  supported  $\text{ZnFe}_2\text{O}_4$  were synthesized using co-precipitation method followed by calcination at 500 °C. The synthesized photocatalysts were characterized using x-ray diffraction (XRD) and scanning electron microscopy (SEM). The synthesized  $\text{ZnFe}_2\text{O}_4$  has low crystallinity. The particle size of  $\text{ZnFe}_2\text{O}_4$  is much smaller than that of the  $\alpha\text{-Al}_2\text{O}_3$  support, and  $\text{ZnFe}_2\text{O}_4$  particles are dispersed on the surface of the crystalline  $\alpha\text{-Al}_2\text{O}_3$  support. 30 wt %  $\text{ZnFe}_2\text{O}_4/\alpha\text{-Al}_2\text{O}_3$  exhibited the highest photocatalytic activity for degradation of methylene blue dye than  $\text{ZnFe}_2\text{O}_4$  and other  $\alpha\text{-Al}_2\text{O}_3$  supported photocatalysts containing 10 wt %, 20 wt % and 40 wt %  $\text{ZnFe}_2\text{O}_4$ . Kinetics of photocatalytic degradation of methylene blue dye using 30 wt %  $\text{ZnFe}_2\text{O}_4/\text{Al}_2\text{O}_3$  obeys Langmuir–Hinshelwood kinetic model. Photocatalytic treatment of real textile wastewater resulted in more effective (when compared to photolytic treatment) in the reduction of wastewater's chemical oxygen demand (COD), pH, conductivity and total dissolved solids (TDS). 30 wt%  $\text{ZnFe}_2\text{O}_4/\text{Al}_2\text{O}_3$  was found to be more effective than unsupported  $\text{ZnFe}_2\text{O}_4$  for the reduction of wastewater's COD, pH, conductivity and TDS.

**Keywords:**  $\text{ZnFe}_2\text{O}_4$ ;  $\alpha\text{-Al}_2\text{O}_3$ ; visible light; methylene blue; textile wastewater

### Introduction

Photocatalysis is an advanced oxidation process that has attracted increasing attention because of its numerous applications in the energy and environmental fields. These applications include: air and water purification, hydrogen generation, self-cleaning of surfaces etc (Yang and Wang, 2018, Nasr *et al.*, 2018, Spasiano *et al.*, 2015).  $\text{TiO}_2$  and  $\text{ZnO}$  are the most widely used photocatalysts due to their nontoxicity, low cost, and good photocatalytic activity. Their major drawback is their high band gaps which makes them to be photocatalytically active only in the presence of ultraviolet light (Bora and Mewada, 2017). The latter constitutes about 5% of the solar spectrum (Casbeer *et al.*, 2012).  $\text{ZnFe}_2\text{O}_4$  is chemically and thermally stable magnetic material that is often used as a visible-light responsive photocatalyst due to its narrow band gap of about 1.9 eV (Zhu *et al.*, 2014, Casbeer *et al.*, 2012) The major technical challenges encountered during application of fine particles of photocatalysts are: aggregation of the fine particles of the photocatalyst which may lead to lower photocatalytic activity, and also the fact that it is often very difficult to separate photocatalyst powder from the reaction medium upon completion of the reaction (Mishra *et al.*, 2018, Srikanth *et al.*, 2017). These challenges trigger the development of various support materials for photocatalysts. Some of the support materials investigated so far include: activated carbon (Jokar-Baloochi *et al.*, 2018), alumina (Ghugal *et al.*, 2017), silica (Meng *et al.*, 2018), zeolites (Ghasemi *et al.*, 2016, Jaafar *et al.*, 2012), clays (Mishra *et al.*, 2018, Mekatel *et al.*, 2012). Aggregation of fine particles of photocatalyst can be

suppressed by dispersing the particles on a suitable support material. Thus, dispersion of  $\alpha$ -Fe<sub>2</sub>O<sub>3</sub> on alumina support improves the photocatalytic activity of  $\alpha$ -Fe<sub>2</sub>O<sub>3</sub> due to reduction in the size of  $\alpha$ -Fe<sub>2</sub>O<sub>3</sub> since the support material prevents growth of  $\alpha$ -Fe<sub>2</sub>O<sub>3</sub> crystals upon heating at higher temperatures required for the synthesis of  $\alpha$ -Fe<sub>2</sub>O<sub>3</sub> (Li *et al.*, 2013). Moreover, Mekatel *et al.* (2012) reported that clay supported narrow band gap semiconductors experience low rate of electron-hole recombination because the support promotes efficient separation of the electron-hole pairs. The low rate of electron-hole recombination enhances the photocatalytic activity of the supported narrow band gap semiconductors.

$\alpha$ -Alumina ( $\alpha$ -Al<sub>2</sub>O<sub>3</sub>) is one of the most widely used support materials for catalysts due to its high specific surface area, low cost, and favorable surface properties (Dorđević *et al.*, 2019, Goudarzi and Salavati-Niasari, 2018, Li *et al.*, 2013). Thus, in terms of photocatalytic activity and stability, alumina was found to be a better support for  $\alpha$ -Fe<sub>2</sub>O<sub>3</sub> photocatalyst than silica (Li *et al.*, 2013). TiO<sub>2</sub>/Al<sub>2</sub>O<sub>3</sub> composite showed improved photocatalytic activity for decomposition of salicylic acid compared to TiO<sub>2</sub> (Anderson and Bard, 1997). Nitrogen-doped TiO<sub>2</sub>/Al<sub>2</sub>O<sub>3</sub> composite was also found to be more active than TiO<sub>2</sub> for photocatalytic degradation of methyl orange (Li *et al.*, 2012). The high photocatalytic activity of TiO<sub>2</sub>/Al<sub>2</sub>O<sub>3</sub> composite was attributed to slow recombination of the photogenerated electrons and holes and the large specific surface area of alumina. Although, there is a lot of work in the literature on the synthesis and photocatalytic activity of ZnFe<sub>2</sub>O<sub>4</sub> and its composites with other semiconductors (Yadav *et al.*, 2018, Behera *et al.*, 2018, Li *et al.*, 2018, Xu *et al.*, 2015), information on supported ZnFe<sub>2</sub>O<sub>4</sub> is scanty in the literature. Therefore, the aims of the present work were to synthesize, characterize and evaluate the photocatalytic activity of ZnFe<sub>2</sub>O<sub>4</sub> on  $\alpha$ -Al<sub>2</sub>O<sub>3</sub> support. The activity of the synthesized photocatalysts was evaluated by monitoring photocatalytic degradation of methylene blue dye (a widely used model for water pollutants) under visible light irradiation.

## Materials and Methods

### Synthesis and characterization of ZnFe<sub>2</sub>O<sub>4</sub>/ $\alpha$ -Al<sub>2</sub>O<sub>3</sub>

Analytical grade reagents (ZnCl<sub>2</sub>.6H<sub>2</sub>O, FeCl<sub>3</sub>.9H<sub>2</sub>O,  $\alpha$ -Al<sub>2</sub>O<sub>3</sub>, NaOH, NaCl) were used in the work. ZnFe<sub>2</sub>O<sub>4</sub> and  $\alpha$ -Al<sub>2</sub>O<sub>3</sub> supported ZnFe<sub>2</sub>O<sub>4</sub> were synthesized using co-precipitation method. ZnCl<sub>2</sub>.6H<sub>2</sub>O and FeCl<sub>3</sub>.9H<sub>2</sub>O in a ratio of 1: 2 were dissolved in distilled water; a solution of NaOH was then added dropwise. The mixed solution was stirred at 70 °C for one hour. The reaction mixture was aged overnight. The solid product was filtered and thoroughly washed with water, dried at 120 °C in an oven, and then calcined in Nabertherm C250 electric furnace at 500°C for two hours to yield ZnFe<sub>2</sub>O<sub>4</sub>.  $\alpha$ -Al<sub>2</sub>O<sub>3</sub> supported ZnFe<sub>2</sub>O<sub>4</sub> were prepared by physical mixing of the desired amounts of  $\alpha$ -Al<sub>2</sub>O<sub>3</sub> and ZnFe<sub>2</sub>O<sub>4</sub> in water. Thus, four different compositions were prepared: 1 g of ZnFe<sub>2</sub>O<sub>4</sub> was mixed with 9 g of  $\alpha$ -Al<sub>2</sub>O<sub>3</sub> to yield 10 wt % ZnFe<sub>2</sub>O<sub>4</sub>/ $\alpha$ -Al<sub>2</sub>O<sub>3</sub>, 2 g of ZnFe<sub>2</sub>O<sub>4</sub> was mixed with 8 g of  $\alpha$ -Al<sub>2</sub>O<sub>3</sub> to yield 20 wt % ZnFe<sub>2</sub>O<sub>4</sub>/ $\alpha$ -Al<sub>2</sub>O<sub>3</sub>, 3 g of ZnFe<sub>2</sub>O<sub>4</sub> was mixed with 7 g of  $\alpha$ -Al<sub>2</sub>O<sub>3</sub> to yield 30 wt % ZnFe<sub>2</sub>O<sub>4</sub>/ $\alpha$ -Al<sub>2</sub>O<sub>3</sub>, and 4 g of ZnFe<sub>2</sub>O<sub>4</sub> was mixed with 6 g of  $\alpha$ -Al<sub>2</sub>O<sub>3</sub> to yield 40 wt % ZnFe<sub>2</sub>O<sub>4</sub>/ $\alpha$ -Al<sub>2</sub>O<sub>3</sub>. The  $\alpha$ -Al<sub>2</sub>O<sub>3</sub> supported ZnFe<sub>2</sub>O<sub>4</sub> samples were dried at 120 °C in an oven. The phase compositions of the synthesized ZnFe<sub>2</sub>O<sub>4</sub> and  $\alpha$ -Al<sub>2</sub>O<sub>3</sub> supported ZnFe<sub>2</sub>O<sub>4</sub> were investigated using powder x-ray diffractometer (Shimadzu, model 6000) with Cu K $\alpha$  radiation (40 kV, 40 mA). The morphology of the synthesized samples was analyzed using Phenom Pro-X desktop scanning electron microscope (SEM).

### Photocatalytic degradation of methylene blue

Photocatalytic experiments were carried out at room temperature (30 $\pm$ 2 °C) using a 500 W halogen lamp as the visible light source. 100 ml of methylene blue solution of a given concentration (25 to 100 mg/L) was mixed with 0.1 g of the photocatalyst in a 250 ml conical flask and stirred for 90 minutes in the dark in order to establish adsorption-desorption equilibrium of methylene blue molecules on the surface of the photocatalyst. The suspension was then exposed to visible light irradiation under continuous stirring at room temperature for one hour. During the irradiation period, samples were periodically taken for analysis after separating the photocatalyst particles. The samples were analyzed for residual concentration of methylene blue using a UV/Vis spectrophotometer at the  $\lambda_{\max}$  of 662 nm. The percentage degradation of methylene blue was calculated using Eq. (1):

$$\text{Degradation} = \frac{(C_0 - C_t)}{C_0} \times 100 \quad (1)$$

where  $C_0$  and  $C_t$  are the initial concentration of methylene blue, and the concentration of methylene blue after irradiation time (t) respectively.

## Photocatalytic treatment of textile wastewater

The textile wastewater used in this study was collected from a textile in Kano city, Nigeria. The wastewater was filtered to remove suspended solids. For photolytic experiments, 100 ml of the textile wastewater was exposed to visible light irradiation at room temperature for 60 minutes. The photolysed sample was then taken for analysis. For photocatalytic experiments, 100 ml of textile wastewater was mixed with 0.1 g of the photocatalyst and stirred for 90 mins in the dark. The suspension was then exposed to visible light irradiation under continuous stirring at room temperature for 60 minutes. The raw and treated textile wastewaters were analyzed for chemical oxygen demand (COD), pH, conductivity and total dissolved solids (TDS) using standard methods (APHA, 1995).

## Results

The XRD patterns of the synthesized  $\text{ZnFe}_2\text{O}_4$  and  $\alpha\text{-Al}_2\text{O}_3$  supported  $\text{ZnFe}_2\text{O}_4$  are shown in Figure 1. The XRD pattern of  $\text{ZnFe}_2\text{O}_4$  displayed in Figure 1a is characterized by broad low intense peaks at Bragg angles of  $31.0^\circ$ ,  $35.1^\circ$ ,  $36.1^\circ$ ,  $42.5^\circ$ ,  $57.2^\circ$  and  $62.5^\circ$  which can be readily assigned to  $\text{ZnFe}_2\text{O}_4$  with cubic phase (JCPDS 01-1109).

Displayed in Figure 2 are the SEM images of  $\text{ZnFe}_2\text{O}_4$  and 30 wt %  $\text{ZnFe}_2\text{O}_4/\alpha\text{-Al}_2\text{O}_3$ . Figure 3 shows the effect of  $\text{ZnFe}_2\text{O}_4$  loading on  $\alpha\text{-Al}_2\text{O}_3$  support and irradiation time on the percentage photocatalytic degradation of methylene blue dye under visible light irradiation. The effect of varying  $\text{ZnFe}_2\text{O}_4$  loading (10, 20, 30 and 40 wt%) on  $\alpha\text{-Al}_2\text{O}_3$  support was investigated at an initial methylene blue concentration of 50 mg/L with a photocatalyst dosage of 1.0 g/L. The effect of initial concentration of methylene blue dye on its photocatalytic degradation using 30 wt %  $\text{ZnFe}_2\text{O}_4/\alpha\text{-Al}_2\text{O}_3$  is presented in Figure 4. The effect of the initial methylene blue dye concentration on its photocatalytic degradation using 30 wt %  $\text{ZnFe}_2\text{O}_4/\alpha\text{-Al}_2\text{O}_3$  was investigated by varying methylene blue concentration from 25 to 100 mg/L. The Langmuir–Hinshelwood kinetic plot for the photocatalytic degradation of methylene blue using 30 wt %  $\text{ZnFe}_2\text{O}_4/\alpha\text{-Al}_2\text{O}_3$  is shown in Figure 5. Table 1 shows the properties of the raw textile effluent and the textile effluent treated via photolysis as well as photocatalysis with  $\text{ZnFe}_2\text{O}_4$  and 30 wt%  $\text{ZnFe}_2\text{O}_4/\alpha\text{-Al}_2\text{O}_3$ .

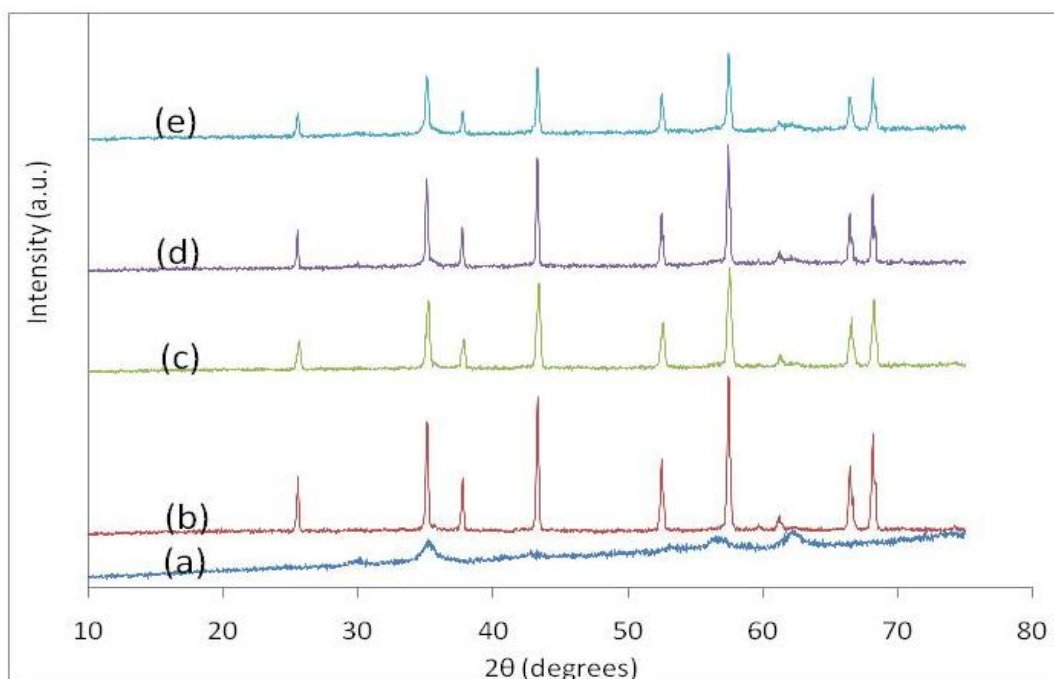


**Figure 1.** XRD patterns of the prepared (a)  $\text{ZnFe}_2\text{O}_4$ , (b) 10 wt %  $\text{ZnFe}_2\text{O}_4/\alpha\text{-Al}_2\text{O}_3$ , (c) 20 wt %  $\text{ZnFe}_2\text{O}_4/\alpha\text{-Al}_2\text{O}_3$ , (d) 30 wt %  $\text{ZnFe}_2\text{O}_4/\alpha\text{-Al}_2\text{O}_3$  and (e) 40 wt %  $\text{ZnFe}_2\text{O}_4/\alpha\text{-Al}_2\text{O}_3$

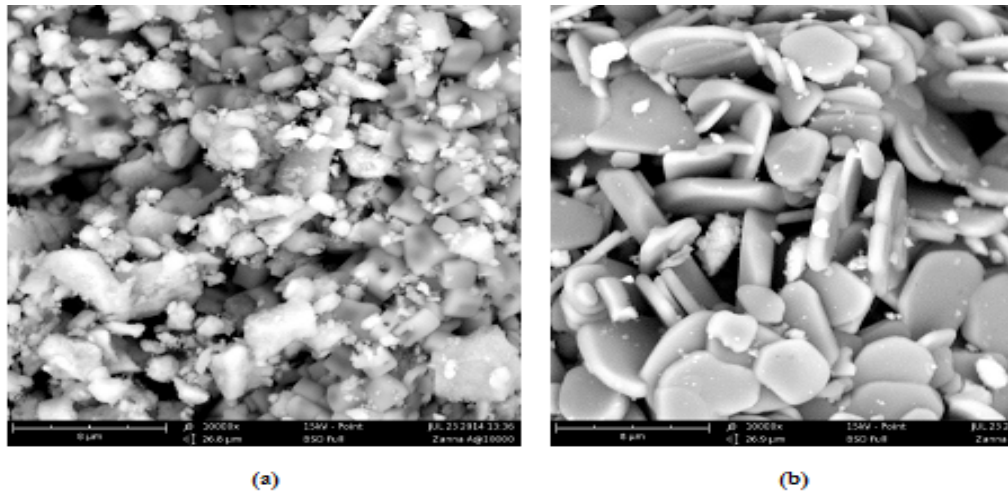


**Figure 2.** SEM images of (a) ZnFe<sub>2</sub>O<sub>4</sub> and (b) 30 wt % ZnFe<sub>2</sub>O<sub>4</sub>/α-Al<sub>2</sub>O<sub>3</sub>

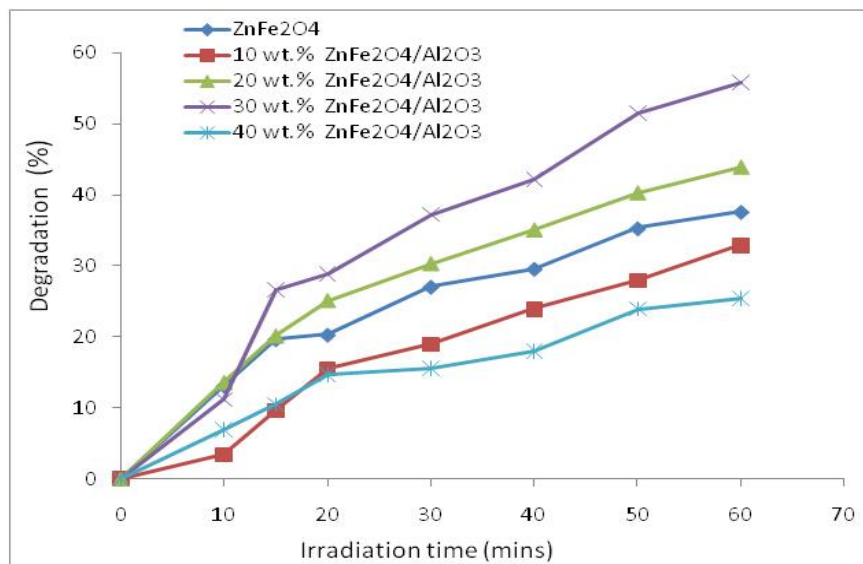


**Figure 3.** Photocatalytic degradation of methylene blue dye using ZnFe<sub>2</sub>O<sub>4</sub> and α-Al<sub>2</sub>O<sub>3</sub> supported ZnFe<sub>2</sub>O<sub>4</sub>

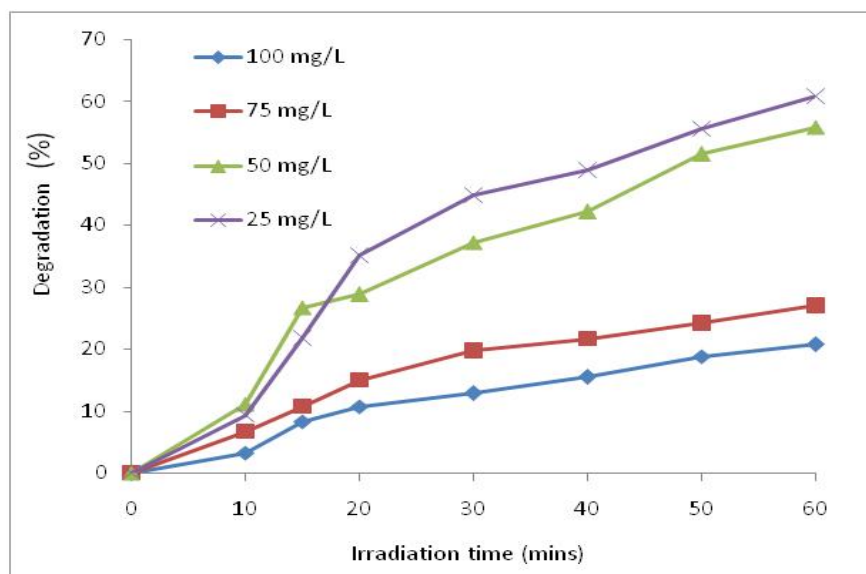


**Figure 4.** Effect of initial concentration of methylene blue on its photocatalytic degradation using 30 wt % ZnFe<sub>2</sub>O<sub>4</sub>/α-Al<sub>2</sub>O<sub>3</sub>

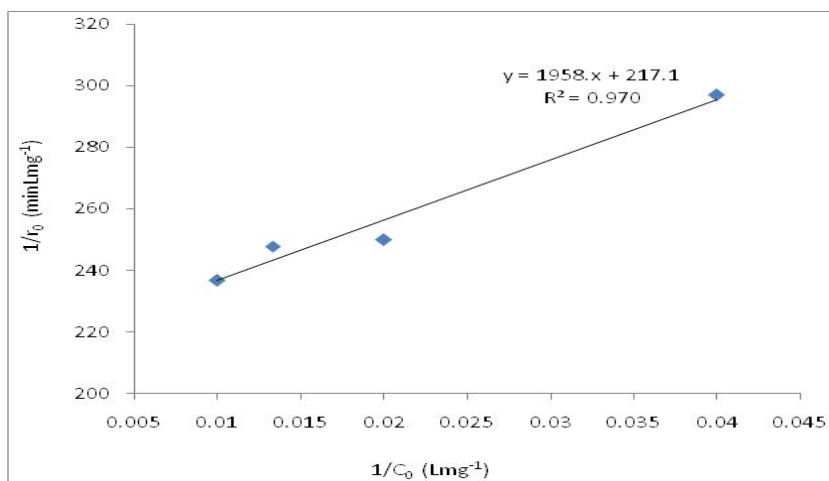


**Figure 5.** Langmuir–Hinshelwood kinetic plot for the photocatalytic degradation of methylene blue using 30 wt % ZnFe<sub>2</sub>O<sub>4</sub>/α-Al<sub>2</sub>O<sub>3</sub>

**Table 1.** Properties of the raw and treated textile effluent

Parameters	Before treatment	After treatment via		
		Photolysis	photocatalysis with ZnFe <sub>2</sub> O <sub>4</sub>	photocatalysis with 30 wt% ZnFe <sub>2</sub> O <sub>4</sub> /α-Al <sub>2</sub> O <sub>3</sub>
COD (mg/L)	784	688	576	416
TDS (mg/L)	982	974	965	949
pH	8.65	8.61	8.49	8.23
Conductivity (μs/cm)	1966	1940	1928	1894

## Discussions

### Characterization of the synthesized ZnFe<sub>2</sub>O<sub>4</sub> and α-Al<sub>2</sub>O<sub>3</sub> supported ZnFe<sub>2</sub>O<sub>4</sub>

The broad peaks are due to the low crystallinity of the prepared ZnFe<sub>2</sub>O<sub>4</sub> at 500 °C. The calcination temperature of 500 °C was selected based on the work of Jadhav *et al.* (2011) which established that ZnFe<sub>2</sub>O<sub>4</sub> sintered at 500 °C shows the highest photocatalytic activity compared to other ZnFe<sub>2</sub>O<sub>4</sub> samples sintered at higher temperatures. Higher sintering temperatures lead to increase in the crystal size of materials thereby decreasing their specific surface areas. As a heterogeneous process, the efficiency of photocatalysis increases as the specific surface area of the photocatalyst is increased. The XRD patterns of α-Al<sub>2</sub>O<sub>3</sub> supported ZnFe<sub>2</sub>O<sub>4</sub> features sharp peaks at 25.85°, 35.41°, 43.62° and 57.76° due to α-Al<sub>2</sub>O<sub>3</sub> (JCPDF 75-1862). ZnFe<sub>2</sub>O<sub>4</sub> peaks are hardly seen in the XRD patterns of the α-Al<sub>2</sub>O<sub>3</sub> supported ZnFe<sub>2</sub>O<sub>4</sub> due to low crystallinity of the synthesized ZnFe<sub>2</sub>O<sub>4</sub>. The Bragg angles of α-Al<sub>2</sub>O<sub>3</sub> peaks did not change after loading with ZnFe<sub>2</sub>O<sub>4</sub>; hence, the crystal structure of the α-Al<sub>2</sub>O<sub>3</sub> supported ZnFe<sub>2</sub>O<sub>4</sub> remained unperturbed after ZnFe<sub>2</sub>O<sub>4</sub> loading.

The SEM images presented in Figure 2a shows that ZnFe<sub>2</sub>O<sub>4</sub> particles are irregularly shaped with particle size in the submicron range. As apparent in Figure 2b, the α-Al<sub>2</sub>O<sub>3</sub> support has a disc like shape with particle size (diameter) of 2–5 μm, and the ZnFe<sub>2</sub>O<sub>4</sub> particles are dispersed on the surface of the α-Al<sub>2</sub>O<sub>3</sub> support. The sizes of ZnFe<sub>2</sub>O<sub>4</sub> particles are very small compared to those of the α-Al<sub>2</sub>O<sub>3</sub> support. Indeed, the SEM images confirm the findings from the XRD data that ZnFe<sub>2</sub>O<sub>4</sub> loading does not alter the crystal structure of the α-Al<sub>2</sub>O<sub>3</sub> support.

### Photocatalytic degradation of methylene blue dye using ZnFe<sub>2</sub>O<sub>4</sub> and ZnFe<sub>2</sub>O<sub>4</sub>/α-Al<sub>2</sub>O<sub>3</sub>

The effect of varying ZnFe<sub>2</sub>O<sub>4</sub> loading (10, 20, 30 and 40 wt%) on α-Al<sub>2</sub>O<sub>3</sub> support was investigated at an initial methylene blue concentration of 50 mg/L with a photocatalyst dosage of 1.0 g/L. It is clearly seen from Figure 3 that the percentage photocatalytic degradation of the dye increases with increase in the ZnFe<sub>2</sub>O<sub>4</sub> loading from 10 wt% to 30 wt% due to the increase in the number of ZnFe<sub>2</sub>O<sub>4</sub> active sites on the α-Al<sub>2</sub>O<sub>3</sub> support. However, photocatalytic degradation of methylene blue decreased when ZnFe<sub>2</sub>O<sub>4</sub> loading was increased to 40 wt%. The observed reduction of the photocatalytic activity of the sample containing 40 wt % ZnFe<sub>2</sub>O<sub>4</sub> can be attributed to the greater agglomeration of ZnFe<sub>2</sub>O<sub>4</sub> particles on α-Al<sub>2</sub>O<sub>3</sub>, thereby

decreasing the rate of diffusion of electron-hole pairs onto the methylene blue dye molecules at the interface of solid photocatalyst-methylene blue dye solution. Retardation of the diffusion of electron-hole pairs decreases the extent of photocatalytic degradation (Li *et al.*, 2013). Agglomeration of ZnFe<sub>2</sub>O<sub>4</sub> particles on the surface of  $\alpha$ -Al<sub>2</sub>O<sub>3</sub> hinders light penetration for an efficient photocatalytic degradation. Similar observations were reported for photocatalytic degradation of methyl orange and Orange II dyes on supported  $\alpha$ -Fe<sub>2</sub>O<sub>3</sub> photocatalysts. Thus, 5 wt%  $\alpha$ -Fe<sub>2</sub>O<sub>3</sub>/zeolite-HY showed the highest activity for degradation of methyl orange (Jaafar *et al.*, 2012), and 25 wt% Fe<sub>2</sub>O<sub>3</sub>/alumina exhibited the highest activity for degradation of Orange II dye (Li *et al.*, 2013). In the present work, highest photocatalytic degradation of methylene blue was achieved with 30 wt % ZnFe<sub>2</sub>O<sub>4</sub>/ $\alpha$ -Al<sub>2</sub>O<sub>3</sub>. As can be seen from Figure 3, the photocatalytic activity of the unsupported ZnFe<sub>2</sub>O<sub>4</sub> is higher than those of 10 wt % ZnFe<sub>2</sub>O<sub>4</sub>/ $\alpha$ -Al<sub>2</sub>O<sub>3</sub> and 40 wt % ZnFe<sub>2</sub>O<sub>4</sub>/ $\alpha$ -Al<sub>2</sub>O<sub>3</sub>, but lower than those of 20 wt % ZnFe<sub>2</sub>O<sub>4</sub>/ $\alpha$ -Al<sub>2</sub>O<sub>3</sub> and 30 wt % ZnFe<sub>2</sub>O<sub>4</sub>/ $\alpha$ -Al<sub>2</sub>O<sub>3</sub>. Therefore, the optimum loading of ZnFe<sub>2</sub>O<sub>4</sub> on the  $\alpha$ -Al<sub>2</sub>O<sub>3</sub> support is a tradeoff between good dispersion of ZnFe<sub>2</sub>O<sub>4</sub> on the support and the amount of the photocatalytically active sites. Moreover,  $\alpha$ -Al<sub>2</sub>O<sub>3</sub> support improves formation of hydroxyl radicals by the photocatalysts (Fu *et al.*, 2012).

### Kinetics of photocatalytic degradation of methylene blue dye using 30 wt % ZnFe<sub>2</sub>O<sub>4</sub>/ $\alpha$ -Al<sub>2</sub>O<sub>3</sub>

The effect of the initial methylene blue dye concentration on its photocatalytic degradation using 30 wt % ZnFe<sub>2</sub>O<sub>4</sub>/ $\alpha$ -Al<sub>2</sub>O<sub>3</sub> was investigated by varying methylene blue concentration from 25 to 100 mg/L. Figure 4 shows that the photocatalytic degradation decreased with increasing initial concentration of methylene blue. For instance, when the initial concentration of methylene blue was increased from 25 to 100 mg/L, the photocatalytic degradation decreased from 68 % to 22 %, after 60 min of visible light irradiation. This observation can be explained as follows: the generation of electrons and holes is the same for a given dosage of photocatalyst and intensity of the incident radiation. At higher initial concentrations, methylene blue molecules can absorb some of the incident visible light. This will decrease the amount of the visible light photons that will drive the photocatalytic process (Jaafar *et al.*, 2012, Konstantinou and Albanis, 2004).

Photocatalytic degradation of the dye was fitted to the Langmuir–Hinshelwood kinetic model which accounts for the photochemical reactions taking place at the interface of solid photocatalyst–liquid substrate solution. The model considers a multi-step reaction mechanism comprising adsorption, photochemical reaction and desorption. The linearized form of the model is given by Eq. 2 (Ounnar *et al.*, 2016, Jaafar *et al.*, 2012).

$$\frac{1}{r_0} = \frac{1}{k_r K_e C_0} + \frac{1}{k_r} \quad (2)$$

where  $r_0$  is the initial reaction rate,  $C_0$  is the initial concentration of methylene blue,  $k_r$  is the intrinsic photocatalytic reaction rate constant ( $\text{mg l}^{-1} \text{min}^{-1}$ ) and  $K_e$  is the adsorption equilibrium constant. The initial reaction rates were derived from Figure 4 at various initial concentrations of the dye. As shown in Figure 5, the kinetic data nicely fitted the Langmuir–Hinshelwood kinetic model with  $R^2$  of 0.970. The calculated values of  $k_r$  and  $K_e$  are  $0.005 \text{ mg l}^{-1} \text{min}^{-1}$  and  $0.111 \text{ mg}^{-1}$ , respectively. Photochemical reaction is the rate determining step of the process because the value of  $k_r$  is smaller than that of  $K_e$ .

### Photocatalytic treatment of textile effluent using ZnFe<sub>2</sub>O<sub>4</sub> and 30 wt % ZnFe<sub>2</sub>O<sub>4</sub>/ $\alpha$ -Al<sub>2</sub>O<sub>3</sub>

The properties of the raw treated textile effluent used in the work are presented in Table 1. Also presented in the Table are the properties of the treated textile effluent via photolysis as well as photocatalysis with ZnFe<sub>2</sub>O<sub>4</sub> and 30 wt% ZnFe<sub>2</sub>O<sub>4</sub>/ $\alpha$ -Al<sub>2</sub>O<sub>3</sub>. Due to the complicated nature of most industrial wastewaters, the organic content of the effluents is measured using lump parameters such as chemical oxygen demand (COD) (Danwittayakul *et al.*, 2015). Irradiation of textile effluent for 60 minutes in the absence of photocatalysts (photolysis) resulted in the COD removal of only 12 % (from 784 to 688 mg/l), this indicates that the organic load of the textile effluent irradiated without photocatalyst did not undergo much change, and the small COD removal observed was due to the photochemical oxidation of various organic compounds present in the wastewater. When the same textile wastewater was exposed to visible light irradiation in the presence of ZnFe<sub>2</sub>O<sub>4</sub> and 30 wt% ZnFe<sub>2</sub>O<sub>4</sub>/ $\alpha$ -Al<sub>2</sub>O<sub>3</sub> for 60 minutes, 27% (from 784 to 576 mg/l) and 47% (from 784 to 416 mg/l) COD removal was achieved, respectively. This shows that 30 wt% ZnFe<sub>2</sub>O<sub>4</sub>/ $\alpha$ -Al<sub>2</sub>O<sub>3</sub> has better photocatalytic performance than the bare ZnFe<sub>2</sub>O<sub>4</sub> for the treatment of the textile effluent.

Conductivity and TDS indirectly measure the amount of inorganic species (such as dissolved salts) in

the effluent. As seen in Table 1. Upon photolysis of the effluent, smaller changes were observed in the properties of the effluent when compared with photocatalysis. This observation can be attributed to more efficient degradation of the organic and inorganic pollutants present in the effluent via photocatalysis. The decrease in the effluent's pH is due to release of CO<sub>2</sub> during photocatalytic degradation of organic pollutants (Konstantinou and Albanis, 2004). The observed reduction of the effluent's conductivity and TDS can be attributed to photocatalytic decomposition of inorganic and organometallic dyes and other pollutants present in the effluent.

## Conclusions

The crystallinity of the synthesized ZnFe<sub>2</sub>O<sub>4</sub> is very low. The size of ZnFe<sub>2</sub>O<sub>4</sub> particles is smaller than that of the  $\alpha$ -Al<sub>2</sub>O<sub>3</sub> support. ZnFe<sub>2</sub>O<sub>4</sub> particles are dispersed on the surface of the  $\alpha$ -Al<sub>2</sub>O<sub>3</sub> support.  $\alpha$ -Al<sub>2</sub>O<sub>3</sub> support improves the photocatalytic activity of ZnFe<sub>2</sub>O<sub>4</sub> under visible light irradiation, and the optimum loading of ZnFe<sub>2</sub>O<sub>4</sub> on  $\alpha$ -Al<sub>2</sub>O<sub>3</sub> is 30 wt %. Photocatalytic degradation of methylene blue dye using 30 wt % ZnFe<sub>2</sub>O<sub>4</sub>/ $\alpha$ -Al<sub>2</sub>O<sub>3</sub> obeys the Langmuir–Hinshelwood kinetic model (R<sup>2</sup>=0.970). The intrinsic photocatalytic reaction rate constant is 0.005 mgL<sup>-1</sup>min<sup>-1</sup>, and the adsorption equilibrium constant is 0.111 Lmg<sup>-1</sup>. Photocatalytic treatment of real textile wastewater resulted in more effective (when compared to photolytic treatment) in the reduction of wastewater's, COD, pH, conductivity and TDS.

## References

- Anderson, C., Bard, A. J. 1997. Improved photocatalytic activity and characterization of mixed TiO<sub>2</sub>/SiO<sub>2</sub> and TiO<sub>2</sub>/Al<sub>2</sub>O<sub>3</sub> materials. *The Journal of Physical Chemistry B*, 101: 2611-2616.
- APHA, 1998. Standard methods for the examination of water and wastewater, 20.
- Behera, A., Kandi, D., Majhi, S. M. 2018. Facile synthesis of ZnFe<sub>2</sub>O<sub>4</sub> photocatalysts for decolourization of organic dyes under solar irradiation. *Beilstein journal of nanotechnology*, 9(1): 436-446.
- Bora, L. V., Mewada, R. K. 2017. Visible/solar light active photocatalysts for organic effluent treatment: Fundamentals, mechanisms and parametric review. *Renewable and Sustainable Energy Reviews*, 76: 1393-1421.
- Casbeer, E., Sharma, V. K., Li, X.-Z. 2012. Synthesis and photocatalytic activity of ferrites under visible light: A review. *Separation and Purification Technology*, 87: 1-14.
- Danwittayakul, S., Jaisai, M., Dutta, J. 2015. Efficient solar photocatalytic degradation of textile wastewater using ZnO/ZTO composites. *Applied Catalysis B: Environmental*, 163: 1-8.
- Dorđević, V., Sredojević, D. N., Dostanić, J., Lončarević, D., Ahrenkiel, S. P., Švrakić, N., Brothers, E., Belić, M., Nedeljković, J. M. 2019. Visible light absorption of surface-modified Al<sub>2</sub>O<sub>3</sub> powders: A comparative DFT and experimental study. *Microporous and Mesoporous Materials*, 273: 41-49.
- Fu, X., Tang, W., Ji, L., Chen, S. 2012. V<sub>2</sub>O<sub>5</sub>/Al<sub>2</sub>O<sub>3</sub> composite photocatalyst: preparation, characterization, and the role of Al<sub>2</sub>O<sub>3</sub>. *Chemical Engineering Journal*, 180: 170-177.
- Ghasemi, Z., Younesi, H., Zinatizadeh, A. A. 2016. Preparation, characterization and photocatalytic application of TiO<sub>2</sub>/Fe-ZSM-5 nanocomposite for the treatment of petroleum refinery wastewater: Optimization of process parameters by response surface methodology. *Chemosphere*, 159: 552-564.
- Ghugal, S. G., Mahalik, R. R., Charde, P. S., Umare, S. S., Kokane, S. B., Sudarsan, V., Sasikala, R. 2017. Photocatalytic properties of mesoporous alumina containing Ni doped CdS nanostructures. *Microporous and Mesoporous Materials*, 242: 284-293.
- Goudarzi, M., Salavati-Niasari, M. 2018. Using pomegranate peel powders as a new capping agent for synthesis of CuO/ZnO/Al<sub>2</sub>O<sub>3</sub> nanostructures; enhancement of visible light photocatalytic activity. *International Journal of Hydrogen Energy*, 43: 14406-14416.
- Jaafar, N. F., Jalil, A. A., Triwahyono, S., Muhid, M. N. M., Sapawe, N., Satar, M. A. H., Asaari, H. 2012. Photodecolorization of methyl orange over  $\alpha$ -Fe<sub>2</sub>O<sub>3</sub>-supported HY catalysts: The effects of catalyst preparation and dealumination. *Chemical engineering journal*, 191: 112-122.
- Jadhav, S. D., Hankare, P. P., Patil, R. P., Sasikala, R. 2011. Effect of sintering on photocatalytic degradation of methyl orange using zinc ferrite. *Materials letters*, 65: 371-373.
- Jokar Baloochi, S., Solaimany Nazar, A. R., Farhadian, M. 2018. 2,4-Dichlorophenoxyacetic acid herbicide photocatalytic degradation by zero-valent iron / titanium dioxide based on activated carbon. *Environmental Nanotechnology, Monitoring and Management*, 10: 212-222.
- Konstantinou, I. K., Albanis, T. A. 2004. TiO<sub>2</sub>-assisted photocatalytic degradation of azo dyes in aqueous solution: kinetic and mechanistic investigations: a review. *Applied Catalysis B: Environmental*, 49: 1-14.

- Li, F.-T., Zhao, Y., Hao, Y.-J., Wang, X.-J., Liu, R.-H., Zhao, D.-S., Chen, D.-M. 2012. N-doped P25 TiO<sub>2</sub>-amorphous Al<sub>2</sub>O<sub>3</sub> composites: One-step solution combustion preparation and enhanced visible-light photocatalytic activity. *Journal of hazardous materials*, 239: 118-127.
- Li, Y., Li, Y., Yin, Y., Xia, D., Ding, H., Ding, C., Wu, J., Yan, Y., Liu, Y., Chen, N., Wong, P. K., Lu, A. 2018. Facile synthesis of highly efficient ZnO/ZnFe<sub>2</sub>O<sub>4</sub> photocatalyst using earth-abundant sphalerite and its visible light photocatalytic activity. *Applied Catalysis B: Environmental*, 226: 324-336.
- Li, Z., Sheng, J., Wang, Y., Xu, Y. 2013. Enhanced photocatalytic activity and stability of alumina supported hematite for azo-dye degradation in aerated aqueous suspension. *Journal of hazardous Materials*, 254: 18-25.
- Mekatel, H., Amokrane, S., Bellal, B., Trari, M., Nibou, D. 2012. Photocatalytic reduction of Cr (VI) on nanosized Fe<sub>2</sub>O<sub>3</sub> supported on natural Algerian clay: characteristics, kinetic and thermodynamic study. *Chemical engineering journal*, 200: 611-618.
- Meng, X., Zhuang, Y., Tang, H., Lu, C. 2018. Hierarchical structured ZnFe<sub>2</sub>O<sub>4</sub>@SiO<sub>2</sub>@TiO<sub>2</sub> composite for enhanced visible-light photocatalytic activity. *Journal of Alloys and Compounds*, 761: 15-23.
- Mishra, A., Mehta, A., Basu, S. 2018. Clay supported TiO<sub>2</sub> nanoparticles for photocatalytic degradation of environmental pollutants: A review. *Journal of Environmental Chemical Engineering*, 6: 6088-6107.
- Nasr, M., Eid, C., Habchi, R., Miele, P., Bechelany, M. 2018. Recent Progress on Titanium Dioxide Nanomaterials for Photocatalytic Applications. *ChemSusChem*, 11(18): 23-3047.
- Ounnar, A., Favier, L., Bouzaza, A., Bentahar, F., Trari, M. 2016. Kinetic study of spiramycin removal from aqueous solution using heterogeneous photocatalysis. *Kinetics and Catalysis*, 57: 200-206.
- Spasiano, D., Marotta, R., Malato, S., Fernandez-Ibañez, P., Di Somma, I. 2015. Solar photocatalysis: Materials, reactors, some commercial, and pre-industrialized applications. A comprehensive approach. *Applied Catalysis B: Environmental*, 170-171: 90-123.
- Srikanth, B., Goutham, R., Badri Narayan, R., Ramprasath, A., Gopinath, K. P., Sankaranarayanan, A. R. 2017. Recent advancements in supporting materials for immobilised photocatalytic applications in waste water treatment. *Journal of environmental management*, 200: 60-78.
- Xu, Q., Feng, J., Li, L., Xiao, Q., Wang, J. 2015. Hollow ZnFe<sub>2</sub>O<sub>4</sub>/TiO<sub>2</sub> composites: High-performance and recyclable visible-light photocatalyst. *Journal of Alloys and Compounds*, 641: 110-118.
- Yadav, N. G., Chaudhary, L. S., Sakhare, P. A., Dongale, T. D., Patil, P. S., Sheikh, A. D. 2018. Impact of collected sunlight on ZnFe<sub>2</sub>O<sub>4</sub> nanoparticles for photocatalytic application. *Journal of colloid and interface science*, 527: 289-297.
- Wang, Z., Li, C., Domen, K., 2018. Recent developments in heterogeneous photocatalysts for solar-driven overall water splitting. *Chemical Society Reviews*, 48(7): 2109-2125.
- Zhu, X., Zhang, F., Wang, M., Ding, J., Sun, S., Bao, J., Gao, C. 2014. Facile synthesis, structure and visible light photocatalytic activity of recyclable ZnFe<sub>2</sub>O<sub>4</sub>/TiO<sub>2</sub>. *Applied Surface Science*, 319: 83-89.